Anisotropic elastic finite-difference modeling of sources and receivers on Lebedev grids

GEOPHYSICS, VOL. 86, NO. 2 (MARCH-APRIL 2021); P. A21–A25, 3 FIGS.
10.1190/GEO2020-0522.1

Anisotropic elastic finite-difference modeling of sources and receivers on Lebedev grids

Erik F. M. Koene[1], Johan O. A. Robertsson[1], and Fredrik Andersson[1]

ABSTRACT

The Lebedev grid finite-difference (FD) method allows modeling of anisotropic elastic-wave propagation. On Lebedev grids, erroneous point-source excitations can create spurious (nonphysical) waves. The only known remedy for such artifacts in the literature is the Lisitsa-Vishnevsky method. This method uses a distributed array to create point sources and point receivers on the FD grid. However, the Lisitsa-Vishnevsky method does not fully eliminate spurious artifacts. A novel approach is found in the FD-consistent point source, which suppresses spurious artifacts entirely. The method requires no array recording to create point receivers. The advantage of this method over the Lisitsa-Vishnevsky method is determined with two anisotropic modeling examples.

INTRODUCTION

Geophysical inversions in anisotropic and complex media require accurate anisotropic modeling methods (Hobro, 2010; Qu et al., 2020). Restricted to staggered-grid finite-difference (FD) methods, we note that the standard Virieux (1986) grid allows an accurate modeling of orthorhombic and higher symmetry media (Hestholm, 2019). However, for lower symmetry media, the Virieux grid ceases to be suitable because strains or strain rates cannot be computed at all required positions. Instead, so-called "fully staggered" or "Lebedev" grids can be used, which are made up of multiple shifted Virieux grids. Examples can be found in electromagnetic (Davydycheva et al., 2003), seismic (Lisitsa and Vishnevsky, 2010; de la Puente et al., 2014), and ultrasonic (Quintanilla and Leckey, 2018) wave modeling.

The numerical (nonphysical) dispersion in Lebedev grids is well studied (Lisitsa and Vishnevsky, 2010; Bernth and Chapman, 2011). However, modeling on Lebedev grids creates an additional nonphysical effect: A point source can excite the correct wavefield as well as multiple spurious wavefields. To suppress such nonphysical wavefields, Lisitsa and Vishnevsky (2010, 2011) suggest to distribute point sources over multiple nodes. Similarly, they suggest to create a point receiver through averaging over multiple nodes. This crucially differs from Virieux grid recordings, in which point receivers are constructed by recording individual nodes. As we will show, the method of Lisitsa and Vishnevsky does not fully suppress the spurious waves.

In this paper, we will show an alternative approach to implement sources and receivers on Lebedev grids using the *FD-consistent* point source derived in Koene et al. (2020a). These point sources are a function of the used FD coefficients, and they undo frequency-dependent amplitude errors induced by the FD simulation. Here, we use FD-consistent point sources for accurate modeling of anisotropic elastic wave propagation on Lebedev grids, without requiring postprocessing at the receiver nodes.

THEORY

Lebedev grid modeling in two dimensions

Consider the velocity-stress system that describes linear elastic wave propagation over time t and space $\mathbf{x} = (x, z)$,

$$\rho \frac{\partial}{\partial t}\begin{bmatrix} v_x(\mathbf{x},t) \\ v_z(\mathbf{x},t) \end{bmatrix} = \begin{bmatrix} \frac{\partial \sigma_{xx}(\mathbf{x},t)}{\partial x} + \frac{\partial \sigma_{xz}(\mathbf{x},t)}{\partial z} \\ \frac{\partial \sigma_{zz}(\mathbf{x},t)}{\partial z} + \frac{\partial \sigma_{xz}(\mathbf{x},t)}{\partial x} \end{bmatrix} + \begin{bmatrix} f_x(\mathbf{x},t) \\ f_z(\mathbf{x},t) \end{bmatrix}, \quad (1)$$

$$\frac{\partial}{\partial t}\begin{bmatrix} \sigma_{xx}(\mathbf{x},t) \\ \sigma_{zz}(\mathbf{x},t) \\ \sigma_{xz}(\mathbf{x},t) \end{bmatrix} = \begin{bmatrix} c_{11} & c_{13} & c_{15} \\ c_{13} & c_{33} & c_{35} \\ c_{15} & c_{35} & c_{55} \end{bmatrix} \begin{bmatrix} \frac{\partial v_x(\mathbf{x},t)}{\partial x} \\ \frac{\partial v_z(\mathbf{x},t)}{\partial z} \\ \frac{\partial v_x(\mathbf{x},t)}{\partial z} + \frac{\partial v_z(\mathbf{x},t)}{\partial x} \end{bmatrix}, \quad (2)$$

Manuscript received by the Editor 4 August 2020; revised manuscript received 14 November 2020; published ahead of production 24 November 2020; published online 05 February 2021.
[1]ETH Zürich, Institute of Geophysics, Zürich 8092, Switzerland. E-mail: erik.koene@erdw.ethz.ch (corresponding author); johan.robertsson@erdw.ethz.ch; fredrik.andersson@erdw.ethz.ch.

where ρ represents the density, v_i represents components of the particle velocity vector, σ_{ij} represents components of the stress tensor, f_i represents components of the external force source, and c_{ij} represents components of the stiffness matrix.

Now define a staggered-grid derivative operator D_x,

$$\mathrm{D}_x q(x) = \sum_{l=1}^{L} \alpha_l \frac{q\left(x + \left(l - \frac{1}{2}\right)\Delta x\right) - q\left(x - \left(l - \frac{1}{2}\right)\Delta x\right)}{\Delta x}, \tag{3}$$

with coefficients α_l chosen subject to $\mathrm{D}_x q(x) \approx \partial q(x)/\partial x$, with spacing Δx. An operator D_z is defined analogously. The Lebedev grid then lays out quantities in space following Figure 1. The superscripts denote whether quantities are located on reference (r) or staggered (s) locations. For example, v_z^{sr} is the vertical particle velocity component that is staggered in the x-direction but not in the z-direction. Then, we replace all spatial derivative operators in equations 1 and 2 with the staggered-grid derivative FD approximation of equation 3. For example, for stresses located at the reference locations, we then write

$$\frac{\partial}{\partial t}\begin{bmatrix}\sigma_{xx}^{rr}(\mathbf{x},t)\\ \sigma_{zz}^{rr}(\mathbf{x},t)\\ \sigma_{xz}^{rr}(\mathbf{x},t)\end{bmatrix} \approx \begin{bmatrix}c_{11} & c_{13} & c_{15}\\ c_{13} & c_{33} & c_{35}\\ c_{15} & c_{35} & c_{55}\end{bmatrix}\begin{bmatrix}D_x v_x^{sr}(\mathbf{x},t)\\ D_z v_z^{rs}(\mathbf{x},t)\\ D_z v_x^{rs}(\mathbf{x},t) + D_x v_z^{sr}(\mathbf{x},t)\end{bmatrix}. \tag{4}$$

We can use a leap-frog time-stepping scheme to step solutions forward in time, and we remove associated errors with time-dispersion transforms (Koene et al., 2018).

The Lisitsa-Vishnevsky source and receiver

Assume that we want to model a directional point-force source

$$\begin{bmatrix}f_x(\mathbf{x},t)\\ f_z(\mathbf{x},t)\end{bmatrix} = \begin{bmatrix}n_x\\ n_z\end{bmatrix}\delta(x - x_s)\delta(z - z_s)S(t), \tag{5}$$

where n_i is a normal vector defining the direction of the source, $\delta(x - x_s)\delta(z - z_s)$ uses Dirac delta distributions to place the source at position $(x, z) = (x_s, z_s)$, and $S(t)$ is a source-time function. Lisitsa and Vishnevsky (2011) show that the Lebedev grid can then produce spurious waves if the source is implemented "wrongly." The solution they propose is to excite the source on the f_i^{rs} and f_i^{sr} grids, with equal strength. The only question remaining, then, is how to implement the spatial point source on both grids. Lisitsa and Vishnevsky (2010, 2011) take a simple approach with respect to this. Take, for example, a source location that is entirely coincident with an f_i^{sr} node. Lisitsa and Vishnevsky propose to excite the f_i^{sr} node fully with, say, a factor one. Additionally, one must excite the source wavelet on the four surrounding f_i^{rs} nodes with a factor of 1/4. Note that this point-source implementation is already described without justification in Davydycheva et al. (2003). We thus refer to this implementation as the Lisitsa-Vishnevsky source.

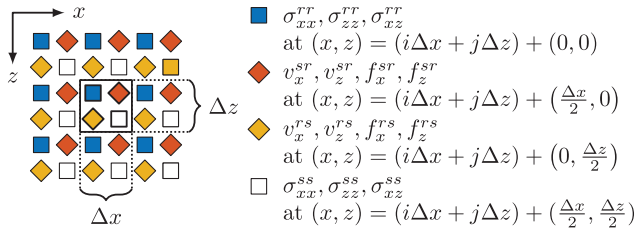

Figure 1. Visualization of nine cells of the 2D Lebedev grid. It is assumed that i and j are integers. Here, for example, (i, j) would take on the values $(1, 2, 3)$.

Lisitsa and Vishnevsky (2010) propose to record waves similarly. Rather than using the field as present on a node, they suggest to use the average on the node, and its four averaged surrounding values, to obtain physically meaningful recordings from the FD simulation.

Lisitsa and Vishnevsky (2010, 2011) suggest this point-source and point-receiver pair only for second-order accurate FD schemes, but it is also used by de la Puente et al. (2014) in an eighth-order accurate FD scheme.

Postulate: FD-consistent modeling of sources and receivers

Following Lisitsa and Vishnevsky (2011), we propose to excite waves on the f_i^{rs} and f_i^{sr} grids. However, we propose two differences. First, we propose to record values as present on the grid, without applying any averaging with surrounding nodes. The idea is that, once the source is excited onto the simulation, all the nodes should contain physically meaningful simulation values, just like typical simulations on Virieux grids. Second, we will use the FD-consistent concept of point sources in FD grids from Koene et al. (2020a).

The idea underlying the FD-consistent point source is that the FD system does not provide solutions to the wave equation. That this is the case is simple to see: Equation 2 does not equal equation 4. Although we carry out FD simulations to obtain solutions to the wave equation, we must be careful not to conflate the two systems. For example, the FD system creates numerical dispersion errors when compared to the wave equation. This means that any concept that applies to the wave equation (such as using a sinc function to represent a band-limited point source; Hicks, 2002) is not always immediately applicable to the FD system. Indeed, a sinc point source can create errors in FD simulations in the form of ringing or even the excitation of wrong wave modes. Examples of such errors may be found in Koene et al. (2020a, 2020b).

The FD system is thus a filtered version of the wave equation. By applying the inverse of this filter to the definition of a point source, we create an FD-consistent point source. This source, when combined with the FD simulation, creates the correct response for a point source for the actual wave equation (except for any remaining numerical dispersion errors). We omit the derivation of the filter and its inverse (which may be found in Koene et al., 2020a), but we give the closed-form solution here. Using a normalized sinc function

$$\mathrm{sinc}(x) \equiv \frac{\sin(\pi x)}{\pi x}, \tag{6}$$

we define the FD-consistent point source for staggered-grid FD operators (for Virieux and Lebedev grids):

$$\delta^{\mathrm{FD}}(x) = \sum_{l=1}^{L} \frac{\alpha_l\left(l - \frac{1}{2}\right)}{\Delta x}\left\{\mathrm{sinc}\left[\frac{x}{\Delta x} - \left(l - \frac{1}{2}\right)\right] + \mathrm{sinc}\left[\frac{x}{\Delta x} + \left(l - \frac{1}{2}\right)\right]\right\}, \tag{7}$$

where α_l are the same FD coefficients as used in equation 3. Note how the FD-consistent point source is a function of the used FD modeling coefficients. A 2D source is created by the product of two 1D sources, that is, $\delta^{\mathrm{FD}}(x)\delta^{\mathrm{FD}}(z)$. The extension to three dimensions follows analogously.

We note four further possibilities that are shown in Koene et al. (2020a) but that are not further discussed here. First, the given FD-consistent point source is potentially nonzero at all nodes of the simulation. This may be undesired in a strongly heterogeneous domain (in Mittet [2002]; however, it is shown that good results with a distributed source are obtained even in heterogeneous domains). A workaround is to use a least-squares or a windowed approximation of the FD-consistent point source, in which fewer nodes are used to mimic the full point-source response. Good results may be obtained using an array with a length equal to that of the FD stencil. Second, the FD-consistent point source may be identically spositioned at locations not coinciding with the grid, at no loss of accuracy. Third, it is also possible to create point-source derivatives (e.g., dipoles) if desired. Finally, we refer to Hicks (2002) for a way to position this distributed source array close to the domain boundaries, which is equally applicable to the FD-consistent point source.

EXAMPLE FOR A TILTED TRANSVERSE ISOTROPIC MODEL

Assume a vertically transverse isotropic (VTI) model with density $\rho = 1000$ kg/m^3 and stiffness matrix

$$\begin{bmatrix} c_{11} & c_{13} & c_{15} \\ c_{13} & c_{33} & c_{35} \\ c_{15} & c_{35} & c_{55} \end{bmatrix}_{\mathrm{VTI}} = \begin{bmatrix} 16.5 & 5.0 & 0 \\ 5.0 & 6.2 & 0 \\ 0 & 0 & 3.7 \end{bmatrix} \text{GPa}. \quad (8)$$

By rotating the symmetry axis 45° counterclockwise from the vertical, a tilted transverse isotropic (TTI) model is found with elasticity constants

$$\begin{bmatrix} c_{11} & c_{13} & c_{15} \\ c_{13} & c_{33} & c_{35} \\ c_{15} & c_{35} & c_{55} \end{bmatrix}_{\mathrm{TTI}} = \begin{bmatrix} 12.1 & 4.2 & -2.6 \\ 4.2 & 12.1 & -2.6 \\ -2.6 & -2.6 & 3.2 \end{bmatrix} \text{GPa}. \quad (9)$$

A directional point-force source is created in the direction perpendicular to the tilted symmetry axis, at $(x, z) = (4005, 4000)$ m, which is coincident with an f_i^{sr} node

$$\begin{bmatrix} f_x(\mathbf{x}, t) \\ f_z(\mathbf{x}, t) \end{bmatrix} = \begin{bmatrix} \cos 45^\circ \\ \sin 45^\circ \end{bmatrix} \delta(x - 4005)\delta(z - 4000)S(t), \quad (10)$$

where the source-time function $S(t)$ is the integral of a 25 Hz Ricker wavelet. We similarly rotate particle velocities in the direction perpendicular to the symmetry axis,

$$V(x, z, t) = \cos(45^\circ)v_x^{sr}(x, z, t) + \sin(45^\circ)v_z^{sr}(x, z, t), \quad (11)$$

which is the quantity that will be plotted in the snapshots. Because the quantities v_x^{sr} and v_z^{sr} are available at coincident locations, no errors are introduced by this rotation. The FD grid is discretized with $\Delta x = \Delta z = 10$ m and $\Delta t = 1$ ms.

TTI model with Taylor coefficients

In our first example, we use the standard Taylor FD coefficients with a half-order $L = 12$ in equation 3. We ran two simulations, one with the Lisitsa-Vishnevsky source and one with the FD-consistent source. Figure 2 shows the results and a close-up of the corresponding source injection terms. The Lisitsa-Vishnevsky source (wherein the source is excited on five nodes) can be clearly recognized. The FD-consistent point source is spread over more nodes. Plotted on

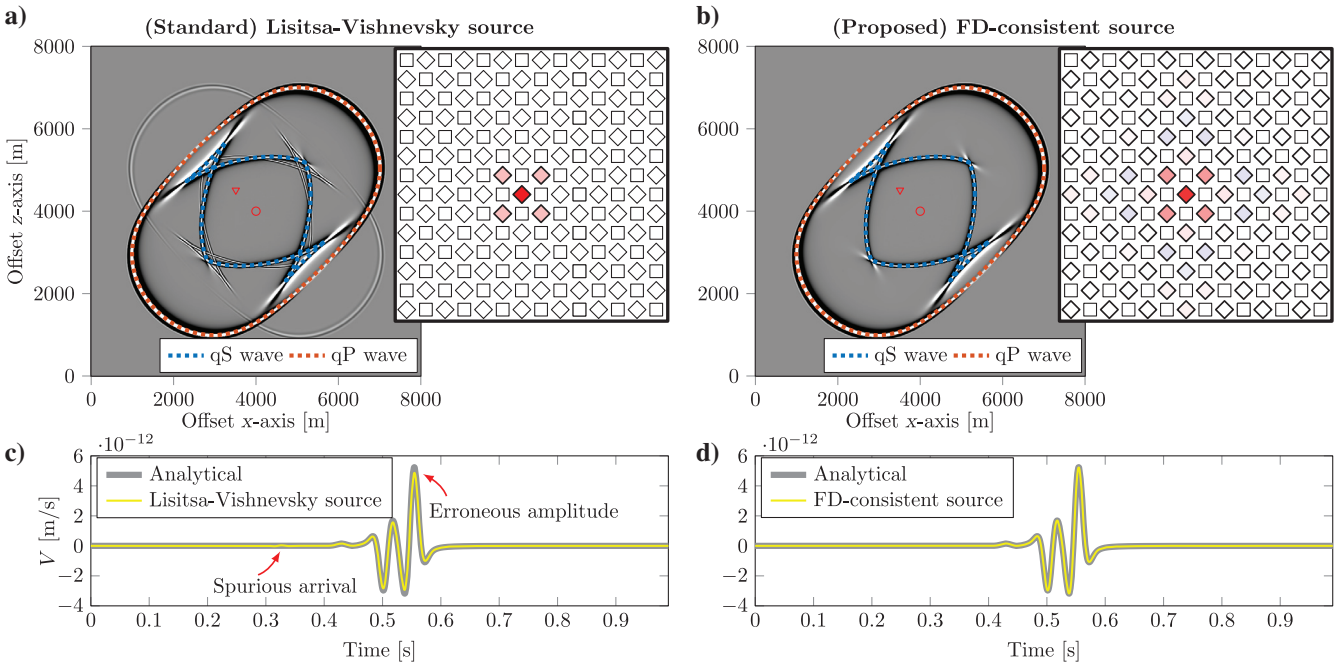

Figure 2. Comparison of two source injection methods in a TTI medium, modeled with Taylor coefficients. (a and b) Snapshots of V, clipped at 1% of the maximum amplitude. A source is denoted by a circle, and a receiver is denoted by a triangle. The magnified diagrams represent the source injection on the Lebedev grid (red = positive, blue = negative). (c and d) The recorded traces corresponding to (a and b), respectively.

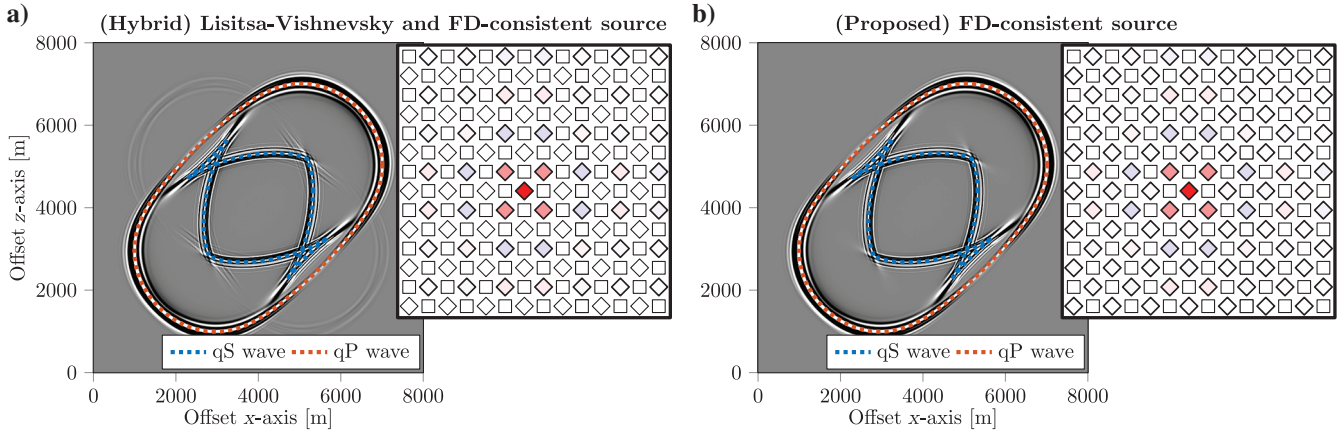

Figure 3. Comparison of two source injection methods in a TTI medium, modeled with least-squares optimal coefficients. (a and b) Snapshots of V, clipped at 1% of the maximum amplitude. The magnified diagrams represent the source-injection on the Lebedev grid (red = positive, blue = negative).

top of the snapshots is the expected location of the qP and qS wavefronts. The Lisitsa-Vishnevsky source generates the desired wave, but it also creates a spurious wavefield. The FD-consistent point source creates no such spurious waves.

Furthermore, we compare the simulations to an analytical solution in Figure 2c and 2d. For this, we recorded V (without averaging) at an offset of $(x, z) = (-500, 500)$ m from the source. The 2D anisotropic analytical solution can be found in Carcione et al. (1988). We observe that the recording due to the Lisitsa-Vishnevsky source contains the spurious arrival and erroneous amplitudes. Note that no form of spatial averaging at the receiver, as proposed by Lisitsa and Vishnevsky (2010), could eliminate these spurious waves. Conversely, the FD-consistent point source excellently matches the analytical solution.

TTI model using high-order optimal FD

In a second example, we again carry out simulations with a half-order $L = 12$ FD operator, but with least-squares optimal coefficients following Liu (2014). We allow a relative phase velocity error of 0.9%, which means that the FD operator will create noticeable wavefield distortions. We choose this coefficient design such that the FD coefficients are significantly different from the Taylor coefficients. The point of the example is not to show which coefficients are superior for modeling. Instead, the point is to show that the FD-consistent point source varies as a function of the FD coefficients. Other model parameters are kept constant.

In the first simulation, we use a "hybrid" source, wherein we use a single-node excitation on one f_i^{sr} node (coincident with the source) and an FD-consistent source on the f_i^{rs} nodes. This source formulation is a hypothetical high-order extension of the Lisitsa-Vishnevsky source. We contrast this to using the FD-consistent source on both grids. Figure 3 shows the results and a close-up of the corresponding source injection terms. We see that the hybrid source still excites spurious wave modes, whereas the full FD-consistent point sources generate no such spurious fields. Clearly, by using the FD-consistent point source on both grids, such artifacts are avoided.

CONCLUSION

In the FD modeling of anisotropic elastic wave propagation on Lebedev grids, spurious modes can be generated by an erroneous implementation of point sources on the FD grid. Typically, such artifacts are suppressed with the Lisitsa-Vishnevsky method, using linear interpolation to implement point sources and point receivers on Lebedev grids. In this paper, we instead propose to use the FD-consistent point source to remove the spurious wave modes. When using the FD-consistent point source, there is no need to average the recordings — the values on the grid provide an excellent fit to an analytical solution. The method comes at a cost of requiring a larger array of nodes into which the source must be injected. Suggestions are given to limit the size of this source array with, for example, a least-squares approximation. We demonstrate that our method works for high-order FD operators with arbitrary FD coefficients. The extension to three dimensions is straightforward.

ACKNOWLEDGMENTS

This work was supported by SNF grant 2-77220-15. We thank J. Hobro, S. Hestholm, an anonymous reviewer, as well as editors J. Blanch, S. de Ridder, and J. Shragge for their helpful and constructive comments on this manuscript.

DATA AND MATERIALS AVAILABILITY

Data associated with this research are available and can be obtained by contacting the corresponding author.

REFERENCES

Bernth, H., and C. Chapman, 2011, A comparison of the dispersion relations for anisotropic elastodynamic finite-difference grids: Geophysics, **76**, no. 3, WA43–WA50, doi: 10.1190/1.3555530.

Carcione, J. M., D. Kosloff, and R. Kosloff, 1988, Wave-propagation simulation in an elastic anisotropic (transversely isotropic) solid: The Quarterly Journal of Mechanics and Applied Mathematics, **41**, 319–346, doi: 10.1093/qjmam/41.3.319.

Davydycheva, S., V. Druskin, and T. Habashy, 2003, An efficient finite-difference scheme for electromagnetic logging in 3D anisotropic inhomogeneous media: Geophysics, **68**, 1525–1536, doi: 10.1190/1.1620626.

de la Puente, J., M. Ferrer, M. Hanzich, J. E. Castillo, and J. M. Cela, 2014, Mimetic seismic wave modeling including topography on deformed staggered grids: Geophysics, **79**, no. 3, T125–T141, doi: 10.1190/geo2013-0371.1.

Hestholm, S., 2019, Elastic tilted orthorhombic (and simpler) wave modeling including free-surface topography: Geophysics, **84**, no. 2, T93–T108, doi: 10.1190/geo2018-0266.1.

Hicks, G. J., 2002, Arbitrary source and receiver positioning in finite-difference schemes using Kaiser windowed sinc functions: Geophysics, **67**, 156–165, doi: 10.1190/1.1451454.

Hobro, J., 2010, Rapid and accurate finite-difference model generation from discontinuous anisotropic velocity models: 80th Annual International Meeting, SEG, Expanded Abstracts, 2961–2965, doi: 10.1190/1.3513461.

Koene, E., J. Robertsson, and F. Andersson, 2020a, A consistent implementation of point-sources on finite-difference grids: Geophysical Journal International, **223**, 1144–1161, doi: 10.1093/gji/ggaa383.

Koene, E. F. M., J. O. A. Robertsson, and F. Andersson, 2020b, A consistent implementation of point-sources on finite-difference grids: 82nd Annual International Conference and Exhibition Workshop Programme, EAGE, Extended Abstracts, 1–5, doi: 10.3997/2214-4609.202011016.

Koene, E. F. M., J. O. A. Robertsson, F. Broggini, and F. Andersson, 2018, Eliminating time dispersion from seismic wave modeling: Geophysical Journal International, **213**, 169–180, doi: 10.1093/gji/ggx563.

Lisitsa, V., and D. Vishnevsky, 2010, Lebedev scheme for the numerical simulation of wave propagation in 3D anisotropic elasticity: Geophysical Prospecting, **58**, 619–635, doi: 10.1111/j.1365-2478.2009.00862.x.

Lisitsa, V., and D. Vishnevsky, 2011, On specific features of the Lebedev scheme in simulating elastic wave propagation in anisotropic media: Numerical Analysis and Applications, **4**, 125–135, doi: 10.1134/S1995423911020042.

Liu, Y., 2014, Optimal staggered-grid finite-difference schemes based on least-squares for wave equation modelling: Geophysical Journal International, **197**, 1033–1047, doi: 10.1093/gji/ggu032.

Mittet, R., 2002, Migration of non-regular data: 72nd Annual International Meeting, SEG, Expanded Abstracts, 1276–1279, doi: 10.1190/1.1816887.

Qu, Y., Z. Guan, J. Li, and Z. Li, 2020, Fluid-solid coupled full-waveform inversion in the curvilinear coordinates for ocean-bottom cable data: Geophysics, **85**, no. 3, R113–R133, doi: 10.1190/geo2018-0743.1.

Quintanilla, F. H., and C. A. Leckey, 2018, Lebedev scheme for ultrasound simulation in composites: Ultrasonics, **86**, 28–40, doi: 10.1016/j.ultras.2018.01.013.

Virieux, J., 1986, P-SV wave propagation in heterogeneous media: Velocity-stress finite-difference method: Geophysics, **51**, 889–901, doi: 10.1190/1.1442147.

Biographies and photographs of the authors are not available.